Available online at www.sciencedirect.com
ScienceDirect
Remote Sensing of Environment 112 (2008) 1450–1463
Remote Sensing of Environment
www.elsevier.com/locate/rse

Variational optimization for global climate analysis on ESA's high performance computing grid

A. Löscher [a,*], C. Retscher [b], L. Fusco [b], P. Goncalves [c], F. Brito [c], G. Kirchengast [d]

[a] GRAS SAF, Danish Meteorological Institute (DMI), Lyngbyvej 100, DK-2100, Copenhagen, Denmark
[b] ESA/ESRIN, Via Galileo Galilei CP 64, 00044 Frascati, Italy
[c] Terradue S.r.l., Via Lunati 10, 00044 Frascati, Italy
[d] Wegener Center for Climate and Global Change (WegCenter) and Institute for Geophysics, Astrophysics, and Meteorology (IGAM), University of Graz, Leechgasse 25, 8010 Graz, Austria

Received 8 September 2006; received in revised form 9 May 2007; accepted 27 May 2007

Abstract

State of the arte assimilation techniques, such as 3D-Var, are relatively seldom used within climate analysis frameworks, partly because of the enormous numerical costs. In order to face this issue ESA's high performance computing Grid on-Demand (G-POD) is used. We assimilate Global Navigation Satellite System (GNSS) based radio occultations (RO). RO data in general exhibit some favorable properties, like global coverage, all-weather capability expected long-term stability and accuracy. These properties and the continuity of data offered by the Meteorological Operational Satellite (MetOp) program and other RO missions are an ideal opportunity to study the long term atmospheric and climate variability.

This paper investigates the assimilation of RO refractivity profiles into first guess fields derived from 21 years of ECMWF's ERA40 dataset on a monthly mean basis divided into four synoptic time layers in order to take the diurnal cycle into account. In contrast to NWP systems, the assimilation procedure is applied without cycling, thus enabling us to run our 3D-Var implementation within G-POD parallel for different time layers. Results indicate a significant analysis increment which is partly systematic, emphasizing the ability of RO data to add independent information to ECMWF analysis fields, with a potential to correct biases. This work lays the ground for further studies using data from existing instruments within a framework based on a mature methodology.

Keywords: Assimilation; Radio occultation; CHAMP; ERA40 climatology; 3D-VAR; Climatology; Climate change; Natural climate variability; Distributed computing; ESA's high performance computing Grid on-Demand

1. Introduction

Climate change is one of the important contemporary issues discussed globally, potentially having a socio-economic and political impact of enormous consequences. Detecting changes and characterizing the natural variability of the global climate system is a major challenge which the atmospheric sciences community will have to face over the next decades. Since there is evidence that the Earth's climate system is influenced by human activities e.g., IPCC (2007) the accurate determination of the atmospheric state is mandatory to monitor and project the evolution of the climate system into the future.

Within the next years assimilation methods will increasingly play an important role in this process due to the broader availability of necessary computing resources and the mutual benefit this methodology is providing by optimization of geophysical information retrieval from different sources. Sources of Earth observation data differ with respect to sampling volume, spectral range, radiative process sensitivity, integration times, geometry, spatial coverage etc., so the combination of data from sources with different properties provides, e.g. significant added value in the sense of global coverage, observations quality control, and consistent observation bias correction procedures (Collard and Healy, 2002). Since the MetOp series of satellites

* Corresponding author.
E-mail address: armin.loescher@uni-graz.at (A. Löscher).

0034-4257/$ - see front matter © 2007 Elsevier Inc. All rights reserved.
doi:10.1016/j.rse.2007.05.022

(operated by EUropean Organisation for the Exploitation of METeorological SATellites (EUMETSAT)) will carry the Global Navigation Satellite System Receiver for Atmospheric Sounding (GRAS), a new state of the art Global Navigation Satellite System (GNSS) based radio occultation (RO) instrument Loiselet et al. (2000), the perspective for a long unbroken chain of globally distributed continuous RO observations of fundamental atmospheric parameters is excellent. The MetOp series of polar satellites Edwards and Pawlak (2000), Silvestrin et al. (2000) is scheduled and financed for a lifetime of 15 years comprising three satellites, the 1st successful launch took place 19, October 2006.

Due to the measurement principle, the RO technique features some preferable characteristics which make it an ideal method for long term monitoring of atmospheric key parameters cf. Anthes et al. (2000), Kirchengast et al. (2000), Leroy and North (2000), Steiner et al. (2001). Global coverage, all weather capability (the signals are not hampered by clouds and precipitation), *a priori* long term stability, and a self-calibrating concept favors its data utilization within frameworks conducting climate studies. The latter property, which distinguishes RO from most other space-borne observational techniques, allows for rather easy inter-comparison of data, offering the opportunity to get a comprehensive data series over decades comprising observations from different receivers and platforms (e.g. Constellation Observing System for Meteorology Ionosphere and Climate COSMIC, which was launched from the Vandenberg Air Force Base, CA, on Friday, April 14. 2006; Rocken et al. (2000)). Problems inherent to other types of remote sensing techniques, like different generations of instruments, calibration problems, and instrumental drift over time cf. Anthes et al. (2000) are mitigated and ease the use of data within assimilation systems. The RO experiment on-board CHAMP, which was launched on July 15, 2000 into a low earth orbit (LEO), provides almost continuously about ~250 globally distributed occultation events per day from which ~170 quality approved atmospheric profiles can be derived since late 2001, (IGAM, geometrical optics processing) Gobiet et al. (2004b), Wickert et al. (2001), Wickert et al. (2004). CHAMP data has been used at the UK Met Office and ECMWF to perform impact studies showing a clearly positive effect on the analyses, despite the limited amount of assimilated observations Healy et al. (2005), Healy and Thepaut (2006). Studies by Foelsche et al. (2003) showed that the sampling error caused by the sparse data flow of one single GPS RO receiver, still allows for accurate global season-to-season temperature climatologies resolving large horizontal scales >1000 km. Nevertheless, with new satellites like MetOp and COSMIC, a broader base of data, which is essential for a better distribution of the local time sampling, can be expected in the near future. These kind of single instrument climatologies have a clear benefit for climate studies, although the data fields might be not consistent due to inadequate coupling of atmospheric parameters. The mix of information comprising unknown error characteristics shall be reduced in order to avoid an increasingly difficult estimation of accuracy. Especially for remote sensing data, where observations are mostly indirect, this criteria of having a pure signal, without additional uncertainty from system inherent errors, is hard to fulfill. RO data itself is closer to an ideal observation for technical reasons compared to most other observations from space-borne instruments. To convert raw observed data into useful variables for the majority of scientists processing steps assuming local spherical symmetry have to be performed. In the future one can probably think of the use of parameters like bending angles or refractivity Leroy et al. (2006) best suited to detect changes of the climate system. In our case statistical optimization and high altitude initialization are used Sokolovskiy and Hunt (1996). This additional information introduced within the retrieval process at high altitudes is only propagated in negligible quantities down to the altitude region of interest. On the other hand reanalysis exercises like ERA40 Kållberg et al. (2004) or NCEP-NCAR 50 Years Reanalysis Kistler et al. (2001) which deliver consistent fields and mitigate the problem caused by the changes and developments within the model itself over the years by freezing the model version and rerun it with the data over large time frames, have proven to be problematic in showing trends and the temporal evolution of the climate system Bengtsson et al. (2004). These problems are mostly caused by the change in the observation systems (new instruments, different generations of instruments, and change of the sensitivity over time due to the space environment and calibration issues).

In order to ease the error characterization and to avoid a possible contamination reducing the information content, observations used in data assimilation systems should be as raw and unprocessed as possible. Obviously there are limits, mostly caused by the complexity of the observation operator, which relates the observed quantity to the control variables, One has either find justified simplification and/or apply some pre-processing steps prior to assimilation to cut down the numerical cost. As we can see, both approaches use raw observation for almost the same reason. Assimilation systems couple the observed physical quantities at different processing levels directly via the observation operator to the atmospheric parameters of the background field.

Single or multiple instrument climatologies are derived by processing the observations carefully avoiding any unnecessary introduction of information and interpolation of the results to a grid. In this context the assimilation procedure, if conducted on a suitable grid, directly delivers fields which are due to the analysis process consistent as a whole. This approach has a clear advantage especially if multiple instrument observations are used as input in contrary to the interpolation of processed data onto a grid.

This suggests that the careful use of additional information, namely the background within a 3D-Var scheme is justified and lead to valuable insights of the temporal variations and the evolution of the Earth's climate system. This procedure has to be seen as a compromise between two contrary methods to derive global fields of atmospheric key parameters (single or multiple instruments versus output from NWP's). It provides additional insight and helps to evaluate the results derived by other methodologies.

In general, the use of assimilation techniques within climatological applications is often very costly regarding computing resources. Many years of data from different sources have to be made available. In order to face this issue we make use of ESA's

high performance computing Grid on-Demand offering the opportunity to compute many time windows in parallel. This breaks down the computing time significantly. Grid on-Demand provides an easy to use, very efficient, and highly collaborative tool to faster process and interpret large amounts of Earth observation data. The Grid uses storage and computing elements, which are located in different geographic locations and combines them to a single instrument. The Grid is the perfect tool to sophisticatedly treat scientific applications and results coming from a variety of atmospheric instruments, where single instrument applications are often lacking proper comparison or even validation mechanisms with similar instruments or equivalent data products.

For this study we use CHAMP observations between 5 and 35 km which had been processed by Geo Forschungs Zentrum Potsadam (GFZ) to Level 2 (phase and orbits) and from the Wegener Center for Climate and Global Change (WegCenter) to refractivity (Level 2a).

The first studies show promising results for temperature proving the chosen concept. Taking the limited amount of observations and the conservative approach to describe their error characteristics into account, the shown impact is reasonable and mirrors the structure of the background error especially at southern high latitudes proving the ability to correct shortcomings in the first guess. Nevertheless the error structures have to be studied further and may be relaxed to allow for bigger increments. The impact on water vapor is still unclear since we omit most of the moist part of the atmosphere (cut-off height 5 km). The use of wave optics processed RO data will enable to review the cut-off criteria and assess the impact on the water vapor fields in the near future. Surface pressure shows an expected behavior which depends to a certain extent on the local orography.

In Section 2 a brief description of the used methodology is given and our specific implementation is presented. Section 3 focuses on the used data, their error characteristics and the selected processing (ESA's Grid on-Demand); Section 4 presents the results of our first assimilation experiments and finally Section 5 provides a summary of our findings and an outlook on future developments.

2. Methodology

2.1. 3D variational assimilation

2.1.1. 3D-Var overview

3D-Var is an iterative optimization methodology to combine data of different sources (e.g. NWP model fields and observations) in a statistically optimal way. This technique and its successor 4D-Var, which takes also the time component of the observations into account, is state of the art and successfully used in NWP centers worldwide, to derive initial conditions for the model runs. In 4D-Var the process is more continuous, as in 3D-Var with defined cut-off times for the observations to be used, generating a real initial condition for the next forecast run. An introduction to the assimilation methodology is given in Bouttier and Courtier (1999), Kalnay (2003). In short, the minimization problem for finding a minimum of the cost function $J(\mathbf{x})$ (also called penalty or misfit function) can be expressed as follows:

$$\mathbf{x}_a = \text{Arg min } J, \tag{1}$$

$$J(\mathbf{x}) = J_b(\mathbf{x}) + J_o(\mathbf{x}), \tag{2}$$

$$J(\mathbf{x}) = 1/2\{(\mathbf{x}-\mathbf{x}_b)^T\mathbf{B}^{-1}(\mathbf{x}-\mathbf{x}_b) + (\mathbf{y}-H(\mathbf{x}))^T\mathbf{R}^{-1}(\mathbf{y}-H(\mathbf{x}))\}, \tag{3}$$

$$\nabla J_{xa} = \mathbf{B}^{-1}(\mathbf{x}_a-\mathbf{x}_b) + \mathbf{H}^T\mathbf{R}^{-1}[H(\mathbf{x}_a)-\mathbf{y}] = 0. \tag{4}$$

The observation and the background cost function are denoted by $J_o(\mathbf{x})$ and $J_b(\mathbf{x})$, respectively.

The solution of the minimization problem requires the calculation of the gradient $\nabla J_{\mathbf{x}}$ and can be performed either in terms of full fields $J(\mathbf{x})$ or in terms of analysis of increments

$$\delta\mathbf{x} = \mathbf{x} - \mathbf{x}_b, \tag{5}$$

$$J(\delta\mathbf{x}) = \frac{1}{2}[\delta\mathbf{x}^T\mathbf{B}^{-1}\delta\mathbf{x} + (\mathbf{H}\delta\mathbf{x}-\mathbf{d})^T\mathbf{R}^{-1}(\mathbf{H}\delta\mathbf{x}-\mathbf{d})], \tag{6}$$

$$\mathbf{d} = \mathbf{y} - H(\mathbf{x}_b), \tag{7}$$

$$\nabla J = \mathbf{B}^{-1}\delta\mathbf{x} + \mathbf{H}^T\mathbf{R}^{-1}\mathbf{H}\delta x - \mathbf{H}^T\mathbf{R}^{-1}\mathbf{d}, \tag{8}$$

where the analysis is found by adding the final increment to the first guess

$$\mathbf{x}_a = \mathbf{x}_b + \delta\mathbf{x}_a. \tag{9}$$

$\delta\mathbf{x}_a$ is found by minimizing the cost function (Eq. (6)) using the cost function gradient (Eq. (8)) and a suitable optimization algorithm. The differences $H(\mathbf{x})-H(\mathbf{x}_b)$ may be written $\mathbf{H}\delta\mathbf{x}$ using a linear approximation, where H is the potentially non-linear observation operator, $\mathbf{H}$ the linear approximation (tangent linear operator) of H, $\mathbf{H}^T$ the adjoint operator, $\mathbf{x}$ the atmospheric state vector, $\mathbf{y}$ the observation vector, $\mathbf{R}$ and $\mathbf{B}$ are the observation and background error covariance matrices, respectively. This formulation is still very expensive from a numerical point of view. Here control space transformations are performed, which include preconditioning procedures, in order to get a better posed problem cf. Zupanski (1993), Kozo (1997).

2.2. Specific implementation

2.2.1. Assimilation system setup

In our climate application of the 3D-Var procedure an incremental approach using control space transformations with empirical orthogonal functions (EOF's) and recursive filters was chosen (details on used data and error characteristics cf. Section 3). The dimensions of the background are selected to best fit to the specific application and computational requirements resulting in the use of a GCM compliant Gaussian grid G48 corresponding to 96 latitudes × 192 longitudes. This is equivalent to a grid point spacing of ~208 km at the equator comprising 60 model levels. These hybrid, terrain following σ-levels have a smooth transition to pressure levels with an uppermost level at 0.10 hPa or ~64.56 km. The vertical

coordinate system is available as grid of pressure, geometrical height (over reference ellipsoid) or geopotential height on the ECMWF hybrid levels. For this assimilation experiment geometrical height was used. The spatial horizontal resolution (G48) is well suited for our application and the grid point spacing agrees excellent with the integrating character of the RO technique Wickert (2002) in the horizontal domain. The 24 h of a day are divided into 6 h time windows around 00, 06, 12 and 18 UTC. A separate assimilation run is performed for every single 6 h interval using the appropriate background fields and set of observations. The whole setup is based on the analysis of monthly means, where the background is a monthly mean of the appropriate time layer. Observations within the assimilation time window (±3 h around the analysis time) from the whole month are used.

The control variables used in the assimilation framework are temperature, specific humidity, and surface pressure. Cross correlations between the control variables are assumed to be small enough to be neglected, which gives block-diagonal background covariance matrices. Moreover we assume that the horizontal and vertical correlations are separable. The cost function is minimized by using a routine for Large-scale Bound-constrained or Unconstrained Optimization (L-BFGS-B), an iterative quasi Newton limited memory algorithm based on the Broyden–Fletcher–Goldfarb–Shanno Method Zhu et al. (1995), Nocedal (1996). The approximated Hessian matrix of second derivatives is constructed by analyzing successive gradient vectors, which allows to apply a quasi Newton fitting method. The Hessian Matrix is not computed at any stage, but the assumption of a locally quadratic approximated function around the optimum has to be made.

2.2.2. Control space transformations

For a model state $\mathbf{x}$ with n degrees of freedom (in our case $\sim 2.3 \times 10^6$) minimization of the cost function is numerically costly and can make the problem practically unsolvable for usual n's. One practical solution to this problem is to perform the minimization in a control variable space $\mathbf{v}$ (same dimension as $\mathbf{x}$), which leads to a preconditioning of the problem at the same time Barker et al. (2003) and is given by

$$\mathbf{x} = \mathbf{U}\mathbf{v}. \tag{10}$$

The transformation matrix $\mathbf{U}$ has to be chosen in a way that

$$\mathbf{B} = \mathbf{U}\mathbf{U}^T. \tag{11}$$

In control space $\mathbf{v}$ the number of required minimization calculations is reduced since the problem becomes better posed. The background error covariance matrix in control space approximately satisfies $\mathbf{B}_c = \mathbf{I}$, where $\mathbf{I}$ denotes the identity matrix, hence the problem is effectively preconditioned. In terms of increments the control variable transform can be written as

$$\delta\mathbf{x} = \mathbf{U}\mathbf{v}. \tag{12}$$

There are different ways to specify the transformation

$$\mathbf{v} = \mathbf{U}^{-1}\delta\mathbf{x}. \tag{13}$$

The definition must provide ways to break down the atmospheric state $\mathbf{x}$ in uncorrelated but physical realistic error modes which can be penalized in J_b according to their estimated error magnitude Skamarock et al. (2005), Barker et al. (2004). The control variable transform as expressed in Eq. (12) is in fact composed of a series of operations

$$\delta\mathbf{x} = \mathbf{U}_h\mathbf{U}_v\mathbf{v}, \tag{14}$$

where the subscript h denotes horizontal and v the vertical part of the control space transform. The respective transformations proceed from control to model space but are reversed in the adjoint calculations where $\mathbf{B}$ in expanded form is written as

$$\mathbf{B} = \mathbf{U}_v\mathbf{U}_h\mathbf{U}_h^T\mathbf{U}_v^T. \tag{15}$$

To verify the adjoint code at different levels (single loops and whole modules) the dot-product test had been used, which verifies the adjoint code with respect to the tangent linear model e.g. Kalnay (2003).

2.2.3. Vertical control variable transform

The vertical transform serves to project control variables from model levels onto the weighted eigenvectors of the vertical component of the background error covariance matrix. The vertical covariance matrix $\mathbf{B}_v$ is given as a $k \times k$ positive-definite symmetric matrix where k is equal the number of vertical levels. These are properties which allow to perform an eigenvalue decomposition with a multiplication by the scaling factor P. $\overline{\mathbf{B}}_v$ denotes a latitude dependent domain averaged $\mathbf{B}_v$ (cf. Section 3.3.2).

$$\mathbf{B}_v = P^{-1}\mathbf{E}\boldsymbol{\Lambda}\mathbf{E}^T P^{-1}, \tag{16}$$

$$\overline{\mathbf{B}}_v = \mathbf{E}\boldsymbol{\Lambda}\mathbf{E}^T \tag{17}$$

The inner product P (here used in scalar notation $P=1$) defines a weighted error which could be used to introduce e.g. synoptic dependencies. The columns of the matrix $\mathbf{E}$ are k eigenvectors $\mathbf{e}(m)$ of $\mathbf{B}_v$, which obey the orthogonally relationship

$$\mathbf{E}\mathbf{E}^T = \mathbf{I}. \tag{18}$$

The diagonal matrix $\boldsymbol{\Lambda}$ contains the k eigenvalues $\lambda(m)$ of $\mathbf{B}_v$; this standard theory can be used to define a transform $\mathbf{U}_v\mathbf{v}$ between variables $\delta\mathbf{x}(k)$ on model levels and their projection onto vertical modes m defined by

$$\mathbf{B}_v = \mathbf{U}_v\mathbf{U}_v^T. \tag{19}$$

The comparison of Eqs. (16) and (19) allows deriving

$$\delta\mathbf{x} = \mathbf{U}_v\mathbf{v}_v, \tag{20}$$

$$\delta\mathbf{x} = P^{-1}\mathbf{E}\boldsymbol{\Lambda}^{1/2}\mathbf{v}_v. \tag{21}$$

Eq. (19) can be inserted into the background cost function in control variable space form

$$J_b = \frac{1}{2}\delta\mathbf{x}^T\mathbf{B}_v^{-1}\delta\mathbf{x}, \tag{22}$$

which gives

$$J_b = \frac{1}{2}\mathbf{v}_\mathrm{v}^T\mathbf{v}_\mathrm{v}, \tag{23}$$

$$J_b = \frac{1}{2}\sum_m \mathbf{v}_\mathrm{v}^2(m), \tag{24}$$

for the background cost function and

$$\nabla J_b = v_v, \tag{25}$$

for the calculation of the background gradient. As can be seen here there are several effects of the $\mathbf{U}_\mathrm{v}$ transform.

- The projection onto the uncorrelated eigenvectors of $\mathbf{B}_\mathrm{v}$ leads to significant CPU savings as can be seen easily *via* Eq. (24) in the calculation of the background cost function respectively in the calculation of the background gradient (see Eq. (25)).
- The scaling by the square root of the eigenvalues $\lambda^{1/2}(m)$ serves as a preconditioner.
- The eigenvectors are ordered by the size of their corresponding eigenvalues, meaning that $\lambda(1)$ is the dominant structure where $\lambda(k)$ essentially contains low amplitude noise. One can use this order to filter vertical grid scale noise by neglecting small-scale eigenvalue structures, which contribute little to the total error. Such a filtering is not part of our current implementation.

2.2.4. Horizontal control variable transform

A transformation $\delta\mathbf{x}=\mathbf{U}\mathbf{v}$ is defined which relates the preconditioned control variables $\mathbf{v}$ to the analysis increment $\delta\mathbf{x}$ in model space. The horizontal control variable transform uses the identity

$$\mathbf{B}_\mathrm{h} = \mathbf{U}_\mathrm{h}\mathbf{U}_\mathrm{h}^T, \tag{26}$$

and follows closely the basic description of the vertical control variable transform, but is realized by scaled recursive filters (RF). The RF has to be applied in a non-dimensional space (since the filter coefficients are defined in non-dimensional space)

$$\tilde{\mathbf{v}} = \mathbf{F}^{1/2}\mathbf{v}, \tag{27}$$

where the scaling factors $\mathbf{F}$ contain the grid box areas (planar elements of the horizontal background grid), $\tilde{\mathbf{v}}$ denotes a non-dimensional control space. The relation between the horizontal part of the background error covariance matrix $\tilde{\mathbf{B}}_\mathrm{h}$ and the background error covariance matrix $\tilde{\mathbf{B}}_\mathrm{h}$, where the tilde stands for non-dimensional space, is given by

$$\mathbf{B}_\mathrm{h} = \mathbf{F}^{-1/2}\tilde{\mathbf{B}}_\mathrm{h}\mathbf{F}^{-1/2}. \tag{28}$$

A comparison between Eqs. (26) and (28) indicates that the horizontal component of the control variable transform $\mathbf{U}_\mathrm{h}$ can be represented by using a recursive filter R as

$$\delta\mathbf{x} = \sigma_\mathrm{b}\mathbf{F}^{-1/2}R\mathbf{F}^{1/2}\mathbf{v}, \tag{29}$$

where σ_b is the background standard deviation if not already implicitly applied through the vertical control space transformation (in our case σ_b is used to introduce the surface pressure standard deviation). The basic algorithm for a recursive filter is quite simple. The RF is defined through an initial function A_j at grid points j where $1 \le j \le J$. A single pass of the RF consists of an initial smoothing from *left* to *right*

$$B_j = \alpha B_{j-1} + (1-\alpha)A_j \quad \text{for} \quad j = 1\ldots J, \tag{30}$$

followed by another pass from *right* to *left*

$$C_j = \alpha C_{j+1} + (1-\alpha)B_j \quad \text{for} \quad j = J\ldots 1. \tag{31}$$

The application of the RF in each direction is performed to ensure zero phase change. So a 1-pass filter is defined as a single application of Eqs. (30) and (31), an N-pass RF is defined by N sequential applications of Eqs. (30) and (31). The α denotes the filter coefficients which can be derived in a way, taking the number of filter passes N into account, that the filter output matches analytical functions. For the limit $N\to\infty$ the output of the RF tends to a Gaussian function. In short α is calculated as follows:

$$\frac{\alpha}{(1-\alpha)^2} = \frac{1}{2E}, \tag{32}$$

$$E = \frac{N(\Delta x)^2}{s^2}, \tag{33}$$

where Δx denotes the grid spacing and s the characteristic length scale which can be empirically derived to match given correlations. It follows for α

$$\alpha = 1 + E - \sqrt{E(E+2)}. \tag{34}$$

Finally a scaling factor S has to be defined to conserve the background error variance, for the zero distance case. S is calculated as the inverse of the zero distance response of a one dimensional N-pass RF to a delta function. In consequence of the non-equidistant Gaussian grid α is spatially dependent. A two dimensional RF results by the perpendicular application of a one dimensional RF and the use of S^2 as scaling factor. When the RF is applied within our assimilation framework only $N/2$ passes are performed, as indicated in Eq. (26) the other $N/2$ passes are performed by the adjoint transform. Details concerning RF's and the matching with analytical functions are given in Lorenc (1992), Hayden and Lorenc (1995). In our application we use a six pass filter ($N=6$) which quite accurately resembles a Gaussian function. The filter coefficients A are calculated in a way to approximate the horizontal error structures of the control variables. To avoid a boundary problem (no transfer of information from point 1 to point J and vice versa) the filter is applied twice with a shifted grid arrangement Löscher et al. (2006).

2.2.5. The observation operator

The observation operator as applied within our system to the data introduced in Section 3 consists of the interpolation

procedures and the forward model to convert interpolated state vector quantities to the observed quantity (in our case refractivity). To calculate the background values at the spatial location of the observations two bilinear horizontal and one (linear for temperature, logarithmic for pressure, and specific humidity) vertical interpolations are performed. The σ level pressure grid is first calculated from the surface pressure. As forward model a simplification of the Smith–Weintraub formula (no k_2 term which is small enough for microwave frequencies to be neglected in our application and no terms describing the non-ideal gas as in the Thayer formula) is used so the refractivity forward operator can be written as:

$$N = k_1 \frac{p_A}{T} + k_3 \frac{e}{T^2}. \tag{35}$$

This formulation follows e.g., Kursinski et al. (2000), where N denotes the refractivity, T is the absolute temperature, e is the partial pressure of water vapor, k_1 and k_3 are empirical constants. In order to calculate the corresponding gradients, the adjoint of the observation operator is used, which was partly derived by using TAPENADE (Tangent and Adjoint PENultimate Automatic Differentiation Engine) INRIA (2002) and partly by manual coding. TAPENADE is an automatic code differentiation tool from the Institut National de Recherche en Informatique et en Automatique (INRIA), which is available *via* the web (http://tapenade.inria.fr:8080/tapenade/index.jsp, Aug. 2006).

3. Used data and selected processing

3.1. Grid on-Demand

The European Space Agency (ESA) Science and Application Department of Earth Observation Programmes Directorate at ESRIN has focused on the development of a dedicated Earth Science Grid infrastructure, under the name Earth Observation Grid Processing on-Demand (G-POD). This environment provides an example of transparent, fast, and easy access to data and computing resources. Using a dedicated Web interface, each application has access to the ESA operational catalogue via the ESA Multi-mission User Interface System (MUIS) and to storage elements. It furthermore communicates with the underlying Grid middleware, which coordinates all the necessary steps to retrieve, process, and display the requested products selected from the large database of ESA and third-party missions. This makes G-POD ideal for processing large amounts of data, developing services which require fast production and delivery of results, comparing scientist approaches to data processing and permitting easy algorithm validation Fusco et al. (2007).

While conducting their research, Earth scientists are often hindered by difficulties locating and accessing the right data, products, and other information needed to turn data into knowledge, e.g. interpretation of the available data. Data provision services are far from optimal for reasons related both to science and infrastructure capabilities. The process of identifying and accessing data typically takes up the most time and recourses. Of the different base causes, those most frequently reencountered relate to:

- The physical discontinuity of data.
- The diversity of (meta) data formats.
- The large volume of data.
- The unavailability of historic data.
- The many different actors involved.

At ESA the current functionality in Grid on-Demand Retscher et al. (2006) for atmospheric science purposes provides access to ERS-2 and Envisat atmospheric data, such as the Global Ozone Monitoring Experiment (GOME), the Global Ozone Monitoring by Occultation of Stars (GOMOS), the Michelson Interferometer for Passive Atmospheric Sounding (MIPAS), and the Scanning Imaging Absorption Spectrometer for Atmospheric Cartography (SCIAMACHY). Other Envisat data like the Medium Resolution Imaging Spectrometer (MERIS), the Advanced Along-Track Scanning Radiometer (AATSR), and the Advanced Synthetic Aperture Radar (ASAR) are also available. On Grid there is as well a collection of other satellite data, such as the Meteosat Second Generation (MSG), or Advanced Very High Resolution Radiometer (AVHRR) and Moderate Resolution Imaging Spectroradiometer (MODIS).

For this work we integrated a CHAMP dataset thus opening the door for a new data type coming from RO experiments.

Grid on-Demand not only holds a large amount of data, it moreover stands for distributed computing by offering access to a vast number of computing elements controlled by the user *via* a single website. (cf. http://eogrid.esrin.esa.int, Aug 2006). Grid on-Demand as well offers the access to data and supports applications using ESA toolboxes like the integrated Basic Envisat & ERS-2 Atmospheric Toolbox (BEAT), Basic ERS & Envisat (A)ATSR and MERIS Toolbox (BEAM), and Basic Envisat SAR Toolbox (BEST).

3.2. RO observations

RO observations exhibit a high vertical resolution, which depends to a certain extent on the used retrieval technique, for geometrical optics retrieval roughly 0.5–1.5 km, and a high accuracy from the upper troposphere to the lower stratosphere of <1 K Gobiet et al. (2007). The quality of the retrieved data is foreseen to be further improved by the use of novel algorithms like wave optics methods Gorbunov (2002), Gorbunov and Lauritsen (2004), Jensen et al. (2003), which improve the retrieval quality especially in the troposphere and enables us to process the data within the lower troposphere almost down to the surface at a vertical resolution better than 500 m which will improve our database in terms of numbers and vertical coverage.

3.2.1. Choice of used quantity

It is desirable to use observations as close to the raw state as possible within a data assimilation system Kuo et al. (2000). There are several reasons to do so, first it is in general more

difficult to describe the error characteristics of the observed quantities after several processing steps, which might introduce additional uncertainties and correlations which are hard to determine. Secondly we have to pay attention to the so-called incest problem, a phenomenon caused by the use of background information in observation pre-processing procedures. In that case observations already contain background information prior to the assimilation process. The resulting analysis is artificially drawn closer to the background than is justifiable. For RO data there are three immediate options, first the use of bending angles, second the use of refractivities, and third the use of further processed data like temperature or humidity profiles. Option three is out of discussion since only dry temperature can be retrieved without the use of additional information to solve the temperature humidity ambiguity. This leaves options one and two, where we have chosen to implement an operator based on the assimilation of refractivity data. Refractivity operators already have a successful track record in quasi operational use and proofed to be accurate and computationally inexpensive. The error structures in refractivity space are assumed to be well defined. The use of bending angles potentially has some advantages and is considered as add-on to the current system. Local bending angle operators are computationally feasible, full 2D operators performing ray tracing within the occultation plane are expensive from the computing point of view. Using bending angles reduces the vertical correlation within one observation profile since solving the Abel integral can be omitted, a processing step that has to be performed to derive refractivity which in addition introduces assumptions due to the high altitude initialization. Several types of bending angle operators have been developed and successfully tested.

3.2.2. RO processing and preprocessing

The mathematical theory of data assimilation assumes bias free observations entering an assimilation framework, so pre-processing of the data must assure the removal of any known biases prior to further processing. CHAMP data exhibit a negative refractivity bias of roughly up to 2%, in the amazons region a positive biases exceeding 1% can be observed, within the lower troposphere Beyerle et al. (2006) in general. This study focuses on the use of data between the upper troposphere and the lower stratosphere, a region which is almost bias free, so a bias removal during the observation pre-processing has been omitted; we are using the fraction of data where its quality is best (5–35 km). Since the RO data products consist of profiles with a vertical resolution, which exceeds the vertical resolution of the used hybrid grid by far (300–400 observations within the interesting altitude domain), a data reduction procedure has to be applied prior to assimilation to reduce the numerical cost and to smooth the profile.

The number of observations within single profiles is reduced by a linear averaging procedure in *log* space, taking the spacing of the mean global vertical grid into account. Fig. 1 depicts the strategy to calculate two super observations between two hybrid levels from the CHAMP profiles, which enter the assimilation scheme. Within the pre-processing step, the quality flags of the observations are used to reject as suspicious flagged data. The quality check uses internal and external criteria at different levels of processing to flag data and identify the problem like not enough data or missing reference data.

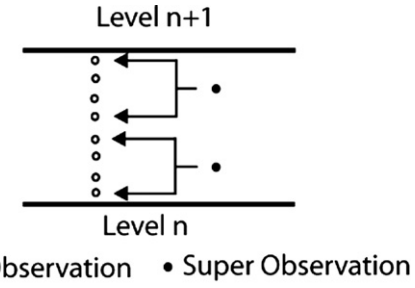

Fig. 1. Schematic representation of the data reduction process.

The purpose of this procedure is on one hand the reduction of the numerical cost and on the other hand a smoothing since the vertical resolution of the observations capture smaller scale atmospheric features than the background grid is capable to do.

The CHAMP data had been processed using the IGAM retrieval scheme Gobiet and Kirchengast (2004a).

3.2.3. RO error characteristics

A simple error covariance matrix formulation was used. Full vertical correlation, no horizontal correlation between the single profiles is assumed since their separation in time and space is sufficient. This formulation was deduced from empirical estimated matrices Steiner and Kirchengast (2005). Similar formulations can be found in Poli et al. (2002) and Healy and Eyre (2000). A least square method was applied to fit analytical functions to the relative standard deviation which shows a different behavior below and above the tropopause. The empirical relative standard deviation can be approximated with an exponential increase above the upper troposphere and lower stratosphere (UTLS) region. Between about 14–20 km it is closely constant, and it can be described with a decrease from near 14 km downwards proportional to an inverse law. To be able to scale the error magnitude, which is receiver dependent, the standard deviation in the UTLS domain (r_{utls}) can be tuned. Eq. (36) gives the analytical functions for the relative standard deviation r_z over all altitude domains, where z denotes the height, z_{Tropotop} the top level of the troposphere domain, $z_{\mathrm{Stratobot}}$ the bottom level of the stratosphere domain and H_{Strato} the scale height of the error increase over the stratosphere.

$$R_z = \begin{cases} r_{\mathrm{utls}} + r_0 \cdot \left[\dfrac{1}{z^p} - \dfrac{1}{z_{\mathrm{Tropotop}}}\right], & \text{for } 2\ \mathrm{km} < z \le z_{\mathrm{Tropotop}} \quad \text{(a)} \\ r_{\mathrm{utls}}, & \text{for } z_{\mathrm{Tropotop}} < z \le z_{\mathrm{Stratobot}} \quad \text{(b)} \\ r_{\mathrm{utls}} \cdot \exp\left[\dfrac{z - z_{\mathrm{Stratobot}}}{H_{\mathrm{Strato}}}\right], & \text{for } z_{\mathrm{Stratobot}} < z \le 50\ \mathrm{km} \quad \text{(c)} \end{cases} \tag{36}$$

To be able to derive the error covariance matrix the correlation length $L(z)$ has to be determined. The best values for $L(z)$ are 2 km within the troposphere (up to ~15 km) and a linear decrease of $L(z)$ above the troposphere to 1 km at 50 km

Table 1
Parameters used to model the CHAMP error characteristics

r_{utls}:	0.5%	z_{Strato}:	15 km
r_0:	4.5%	p:	1.0
$z_{Stratobot}$:	20 km	$L(z)$, 15 km $\leq z$:	Linear decrease to 1 km at 50 km
$z_{Tropotop}$:	14 km	$L(z)$, 2 km $\leq z \leq$ 15 km:	2 km

altitude (details cf. Steiner and Kirchengast (2005)). The observation error covariance matrix **R** can now be described as

$$\mathbf{R} = R_{ij} = r_i r_j \cdot \exp\left(-\frac{|z_i - z_j|}{L(z)}\right). \quad (37)$$

This formulation of the observation error covariance matrix also accounts for the error of representativeness due to its derivation. No additional specification within the assimilation framework is necessary. The values which had been used within this assimilation experiment to describe the error characteristic of CHAMP data are listed in Table 1.

3.2.4. Spatial distribution and temporal sampling

The question of spatial and temporal sampling has to be addressed, since it is impossible to get a really homogenous coverage of the whole globe with one close to polar orbiting satellite (which results e.g. in more profiles at high latitudes than in the tropics and an inhomogeneous local time sampling). For our climate application it is appropriate to focus on seasonal means, a time frame which allows for a sufficient global coverage in space and time by combining the single month analyses (see Fig. 2) Pirscher et al. (2007). Data from COSMIC will significantly improve the inhomogeneous local time sampling present at the moment.

3.3. Background data

3.3.1. First guess fields

Our background data set consists of temperature, specific humidity and surface pressure fields on an ECMWF hybrid grid. To avoid any incest problems, we decided to derive a generic data set from monthly mean ERA40 analysis fields which do not contain RO data. A suitable timeframe to generate first guess fields from this data set are the years 1980 to 2000. This time frame covers a period of increasing and lately massive use of satellite observations, improving the analysis over remote and data sparse areas like the southern hemisphere significantly. This monthly mean fields are averaged separately for the four 6 hours

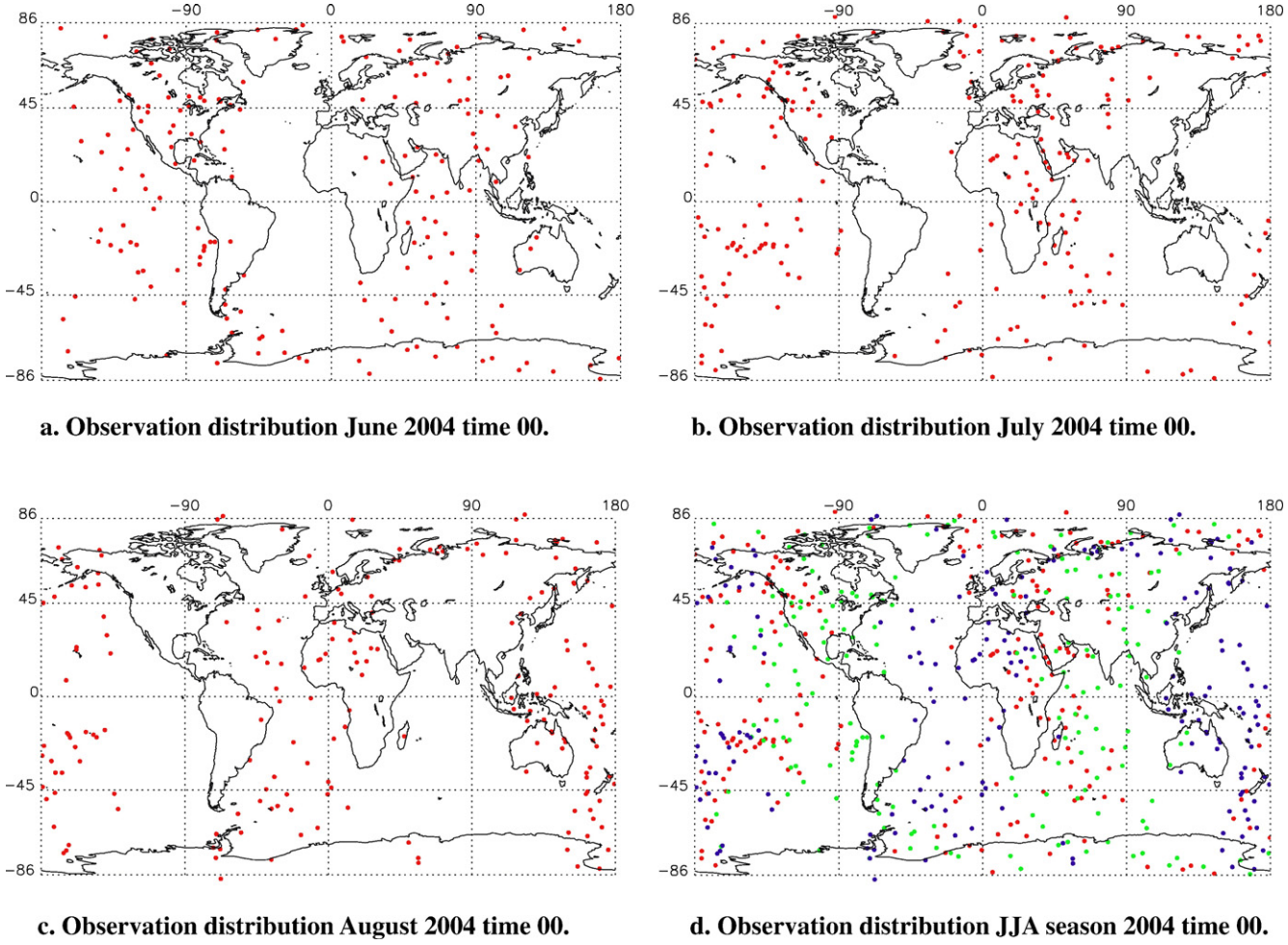

Fig. 2. Observation distribution for the 00 time layers of the JJA season 2004 (a, b, c) and the combined observation distribution of the 00 time layer for the JJA season 2004.

time windows around 00, 06, 12 and 18 UTC. The fields are directly drawn from the ECMWF data archive (Meteorological Archival and Retrieval System MARS) in the used N48 resolution as gridded binary (GRIB) files.

3.3.2. Background error characteristic

Monthly mean error patterns are not readily available and had to be derived (standard methods like e.g. NMC method (Parrish and Derber (1992) can not be used in this context). For this dataset the monthly mean variances of the used atmospheric parameters (temperature, specific humidity and surface pressure) are available from the MARS system too and calculated as follows

$$a_{\mathrm{var}} = \frac{1}{k-1}\sum_{n=1}^{n=k}(a_n - \hat{a})^2, \tag{38}$$

where k denotes the number of days, a_{var} the monthly mean spatially varying variance of a parameter, a the daily analysis value and $\hat{a}$ the corresponding monthly mean. The vertical background correlation matrices of the monthly mean fields are not available and calculated from a subset, namely from the years 1980, 1985, 1990, 1995 and 2000. First the vertical error covariance matrix **B** (where **B** denotes here an error covariance matrix in a general sense) is computed from the differences $\Delta\mathbf{x}_n$ between the monthly mean and the *true values* as which the daily analyses serve, for the k vertical levels.

$$\mathbf{B} = \left[\frac{1}{k-1}\sum_{n=1}^{n=k}(\Delta\mathbf{x}_n)(\Delta\mathbf{x}_n)^T\right] \tag{39}$$

The diagonal elements of **B** represent the variances (B_{ii}) at vertical level i with its non-diagonal elements representing the covariance (B_{ij}) between the vertical levels i and j. From **B** the error correlation matrix $\mathbf{C}_v$ with its elements C_{ij} denoting the error correlations between Δx_i at level i and Δx_j at level j can be derived. $\mathbf{C}_v$ is finally calculated by dividing the covariance B_{ij} by the square root of the product of variances B_{ii} and B_{jj}

$$C_{ij} = \frac{B_{ij}}{\sqrt{B_{ii}B_{jj}}}. \tag{40}$$

This procedure is repeated for every latitude longitude position of the grid. Since the correlations are not uniform over the whole globe the single correlation matrices are averaged separately for five latitude bands. The correlation matrices are setup with 30° bands for northern high, northern mid, equatorial (60°), southern mid, and southern high latitudes.

The final vertical background error covariance matrices of the control variables are composed of the five derived correlation matrices and the global grids of variances. The same averaging procedure in time as used for the first guess fields had been applied to derive the final error characteristics of the control variables. The horizontal correlations which are not latitude dependent are functions of point to point separation which follow roughly the characteristics of the global mean horizontal error correlations in use at ECMWF within the IFC framework at 2003. A similar procedure as to derive the vertical correlations is executed at the moment.

The total background covariance matrix is formed by means of Eq. (15) where the spatially dependent field of variances and the corresponding correlation matrices are used to form the total background covariance matrix.

Table 2
Details CHAMP data JJA 2002, JJA 2003, JJA 2004 and JJA 2005

Time	Number of profiles				Number of pre-processed observations			
	JJA 2002	JJA 2003	JJA 2004	JJA 2005	JJA 2002	JJA 2003	JJA 2004	JJA 2005
00	3213	3619	2905	3372	176509	198859	157757	184794
06	3444	3345	2897	3288	188893	183358	157395	179739
12	3191	3312	2922	3208	175535	181127	159869	175521
18	3507	3422	2849	3307	192268	187823	155596	181558

3.4. Timeframe of the experiment

For this kind of studies the availability and continuity of data is of paramount importance. The northern hemisphere summer season (JJA) from 2004 has been chosen to perform the experiment. The prepared CHAMP data set for the period from 2002–2005 is listed in the following table (Table 2) showing the continuity of the data flow over several years. The number of RO events is in general lower at low latitudes compare to high latitudes, an effect which stems from the orbit characteristic of satellites in a close to polar orbit.

4. Results and discussion

The assimilation results are presented as seasonal zonal mean increments ($\delta\mathbf{x}_a$ in Eq. (9)) for temperature, specific humidity from model level 40 to 10 and as seasonal mean increment for surface pressure. The covered altitude interval is roughly 5 to 37 km since sigma coordinates are terrain following the altitude scale of the plots represents a global mean of the vertical height grid over reference ellipsoid. Refractivity is also shown as an example of our observed variable with the same graphical characteristics as temperature.

We present as an example the 00 time layer of the JJA season 2004, corresponding to the observations shown in Fig. 2. The analyses for other time layers are consistent with the presented results.

4.1. Zonal mean temperature

Fig. 3 shows the zonal mean increment of the temperature analysis where significant patterns of increments are apparent at the southern and less significant at northern high latitudes. Wave like increment structures seen in other assimilation experiments within an operational context Healy and Thepaut (2006) (analysis differences) or in a comparison study of ECMWF analysis and CHAMP data which is based on temperature difference profiles Gobiet and Kirchengast (2004a) are not visible. This difference stems from the

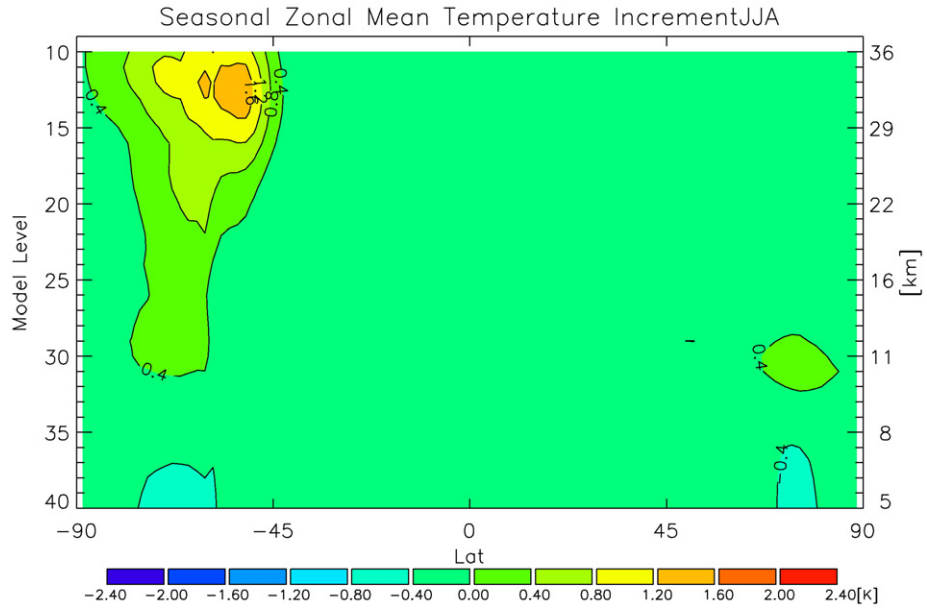

Fig. 3. Zonal mean temperature increment of the 00 time layer of the JJA 2004.

background used in our experiment where the averaging over 21 years of ERA40 data seems to compensate (damping effect due to the averaging process) model shortcomings at the southern high latitudes especially during the (southern) winter season. Similar experiments using short term forecasts and their respective error structures as first guess resulted in increments comparable to Gobiet and Kirchengast (2004a) and Healy and Thepaut (2006). The increment pattern presented here agrees well with the used background temperature error structure indicating a high temperature information content of the observations (cf. Refractivity Section 4.4).

4.2. Zonal mean specific humidity

Since the most water vapor is within the lower troposphere there is not much impact above model level 32 (clearly visible in Fig. 4) which corresponds roughly to 10 km, although it has to be noted that the overall increment is negative. Isolated increments at higher altitudes should be ignored since the system assigns there small numbers and treats them as zero (for initial temperatures below 230 K the system assigns a value of 10^{-12}, the gradients for that values are set automatically to zero, negative humidity values appearing during the minimization

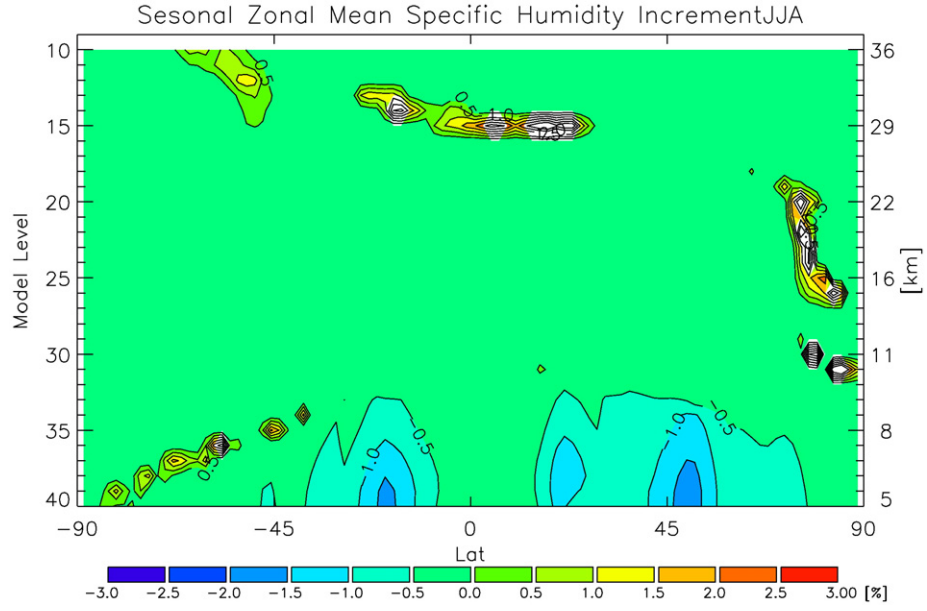

Fig. 4. Zonal mean specific humidity increment of the 00 time layer of the JJA 2004.

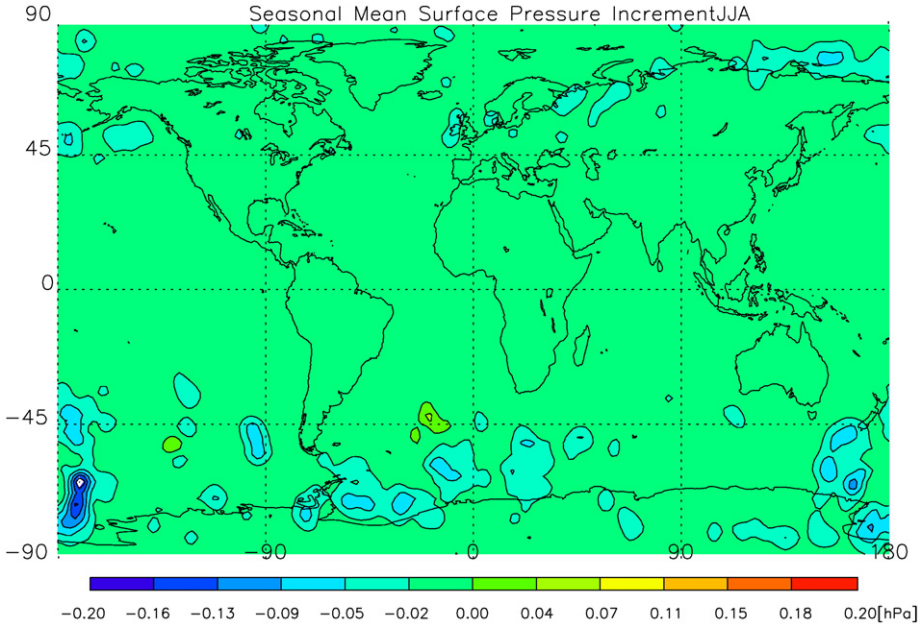

Fig. 5. Surface pressure increment of the 00 time layer of the JJA 2004.

process are subsequently set to 10^{-12}, and treated accordingly). Below level 32 a pattern is apparent but the increment is small compared to the humidity uncertainties of the background. The humidity information content is highest for ray-paths that are close to the surface, these observations are omitted at the moment due to their potential bias.

4.3. Surface pressure

The surface pressure increment shows very pronounced features over Antarctica (see Fig. 5), a phenomenon also observed in the results of other RO assimilation experiments Healy and Thepaut (2006). This might be an effect caused by the special orography of the Antarctic plateau (the magnitude of the increments depends on the distance between the surface and the lowermost observation Palmer et al. (2000), this effect is subject to the specific implementation). The missing increments at low latitudes can be explained by the fact that RO observations around the tropics are harder to retrieve down to the lowermost layers of the atmosphere due to the strong humidity gradients there, new processing techniques (wave optics) are better at coping with this problem.

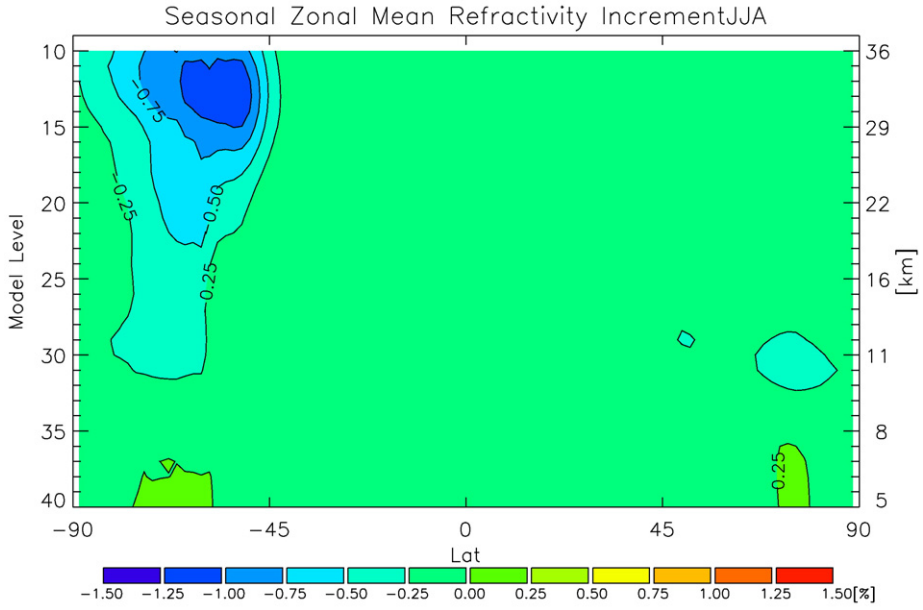

Fig. 6. Zonal mean refractivity increment of the 00 time layer of the JJA 2004.

The use of these methods will enable to review the cut-off criteria in future with considerable impact on the humidity analysis.

4.4. Refractivity

The difference between the refractivity calculated from the first guess data and the analysis is shown in Fig. 6 which mirrors the temperature plot (Fig. 3) with different sign. The interrelationship of these quantities suggests such a result but it also shows that the refractivity is predominantly a function of temperature in our analysis.

5. Summary, conclusions, and outlook

An assimilation scheme was presented using RO data from CHAMP and a first guess derived from ECMWF ERA40 fields for global climate studies. This choice of background information provides us with a versatile dataset based on monthly means which is static and model independent in contrast to dynamic model fields (meaning the operational output of NWP's), where any change in the model will alter the error characteristic. With the static approach no reconsideration of the error derivation is needed. Furthermore we are not affected by a possible incest problem, allowing us to use the whole spectrum of remote sensing data available.

Nevertheless one has to mention that the background might be biased and the analysis thus might carry a signature of that bias, since assimilation systems in general are designed to cope with unbiased observations and background information. Although this poses no problem in itself as long as the time variations under study vary more slowly than the phenomena one wants to capture.

We run the system on ESA's high performance computing Grid on-Demand framework, opening the door for a new observation type and successfully demonstrating the feasibility of assimilation methods for climate studies. Distributed computing is an enabling technology to solve these kind of problems which are demanding in terms of CPU. Since the day is divided in four time layers one year of observations can be processed on a monthly mean base using 48 nodes within approximately 3 – 4 days (the actual computing time depends heavily on the number of used observations and to a certain extent on the load on the grid). Due to the fact that we cut-off the RO profiles at 5 km the impact on the specific humidity and surface pressure analyses is quite limited, temperature and refractivity analyses have the most value. The use of novel retrieval techniques like wave optics processing is expected to change this situation. At the moment we focus on RO data since their inherent properties make them ideal for climate studies, with the launch of COSMIC the number of observation per day multiplied and later this year we expect from the GRAS instrument on-board MetOp data with unprecedented accuracy. Nevertheless the use of complementary observations with high spatial resolution like IASI (Infrared Sounding Interferometer) will be considered for future algorithm enhancements. For validation purposes the obtained analysis should be verified by using *in situ* measurements as a reference.

As a next step the implementation of a bending angle operator is foreseen further reducing the number of pre-processing steps fostering assimilation principles. The presented scheme will be adapted by the GRAS-SAF (GRAS Satellite Application Facility) in future to generate fields based on GRAS data. We successfully showed the relevance of assimilation techniques for climate studies and the feasibility if the necessary computing infrastructure is available. Thus we expect that these techniques will play a more prominent role in future not only in climate applications but also in cross validation activities and bias removal procedures. Balancing the shortcoming of different remote sensing techniques by combining them, results in a product of significant added value reflecting, in an optimal case, only the advantages of the different observations used. These activities will increase our knowledge about the accuracy of remote sensing data sets and might as well be used to consolidate long term records from past decades if complementary information is available, potentially having a profound impact on climate research.

Acknowledgments

The authors want to thank U. Foelsche, A. Gobiet, and M. Borsche (WegCenter, Austria) for providing the processed CHAMP profiles, J. Wickert and T. Schmidt (GFZ, Potsdam, Germany) for making available CHAMP occultation data, A.K. Steiner (WegCenter, Austria) for the provision of the CHAMP error characteristics and M. Fisher (ECMWF, England) for providing input on ECMWF error characteristics. The GRAS-SAF (Global Navigation Satellite-System Receiver for Atmospheric Sounding- Satellite Application Facility, supported by DMI and EUMETSAT), Kent B. Lauritsen and Georg Bergeton Larsen are thanked for enabling this study within a visiting scientist project. The authors are further thankful for fruitful discussions with C. Zehner, S. Casadio, and J. v. Bemmelen (ESA/ESRIN, Frascati, Italy). Moreover we want to acknowledge important contributions from R. Cossu and V. Forneris (ESA/ESRIN, Frascati, Italy).

References

Anthes, R. A., Rocken, C., & Kuo, Y. (2000). Applications of COSMIC to meteorology and climate. *TAO (Terrestrial, Atmospheric and Ocean Sciences)*, *11*(1), 115−156.

Barker, D.M., Huang, W., Guo, Y.-R., & Bourgeois, A.J. (2003). A three-dimensional variational (3DVAR) data assimilation system for use with MM5. NCAR Tech. Note, NCAR/TN-453+ STR, 68 pp. Available from UCAR Communications, P.O. Box 3000, Boulder, CO 80307.

Barker, D. M., Huang, W., Guo, Y. -R., Bourgeois, A. J., & Xiao, Q. N. (2004). A three-dimensional variational data assimilation system for MM5: implementation and initial results. *Monthly Weather Review*, *132*, 897−914.

Bengtsson, L., Hagemann, S., & Hodges, K. I. (2004). Can climate trends be calculated from reanalysis data? *Journal of Geophysical Research*, *109*, D11111. doi:10.1029/2004JD004536

Beyerle, G., Schmidt, T., Wickert, J., Heise, S., Rothacher, M., König-Langlo, G., et al. (2006). Observations and simulations of receiver-induced

refractivity biases in GPS radio occultation. *Journal of Geophysical Research*, *111*, D12101. doi:10.1029/2005JD006673

Bouttier, F., & Courtier, P. (1999). *Data Assimilation Concepts and Methods, Meteorological Training Course Lecture Series.* Shinfield Park, Reading, RG2 9AX, England: European Centre for Medium Range Weather Forecast.

Collard, A. D., & Healy, S. B. (2002). The combined impact of future spaced atmospheric sounding instruments on numeric weather prediction. *Quarterly Journal of the Royal Meteorological Society*, *128*, 1−999.

Edwards, P. G., & Pawlak, D. (2000). MetOp: the space segment for EUMETSAT's polar system. *ESA Bulletin*, *102*, 6−18.

Foelsche, U., Kirchengast, G., & Steiner, A. K. (2003). Global climate monitoring based on CHAMP/GPS radio occultation data. *Proc. Book 1st CHAMP Science Meeting* (pp. 397−407). Heidelberg: Springer-Verlag.

Fusco, L., Cossu, R., & Retshcher, C. (2007). Open Grid Services for Envisat and Earth Observation Applications. In A. J. Plaza & C.-I. Chang (Eds.), *High-performance computing in remote sensing*. Chapman & Hall/CRC Computer and Information Science Series.

Gobiet, A., & Kirchengast, G. (2004). Advancements of Global Navigation Satellite System radio occultation retrieval in the upper stratosphere for optimal climate monitoring utility. *Journal of Geophysical Research*, *109*, D24110. doi:10.1029/2004JD005117

Gobiet, A., Steiner, A. K., Retscher, C., Foelsche, U., & Kirchengast, G. (2004). *Algorithms Validation Based on CHAMP/GPS Data.* Tech. rep., Inst. for Geophys., Asrophys., and Metorol. Austria: Univ. of Graz.

Gobiet, A., Kirchengast, G., Manney, G. L., Borsche, M., Retscher, C., & Stiller, G. (2007). Retrieval of temperature profiles from CHAMP for climate monitoring: Intercomparison with Envisat MIPAS and GOMOS and different atmospheric analyses. *Atmospheric Chemistry and Physics Discussions*, *7*, 3519−3536.

Gorbunov, M. E. (2002). Canonical transform method for processing radio occultation data in the lower troposphere. *Radio Science*, *37*, 1076. doi:10.1029/2000RS002592

Gorbunov, M. E., & Lauritsen, K. B. (2004). Analysis of wave fields by Fourier integral operators and their application for radio occultations. *Radio Science*, *39*, RS4010. doi:10.1029/2003RS002971

Hayden, C. M., & Lorenc, A. C. (1995). Recursive filter for objective analysis of meteorological fields. Applications to NESDIS operational processing. *Journal of Applied Meteorology*, *34*, 3−15.

Healy, S. B., & Eyre, J. R. (2000). Retrieving temperature, water vapour and surface pressure information from refractive-index profiles derived by radio occultation: a simulation study. *Quarterly Journal of the Royal Meteorological Society*, *126*, 1661−1683.

Healy, S. B., & Thepaut, J. -N. (2006). Assimilation experiments with CHAMP GPS radio occultation measurements. *Quarterly Journal of the Royal Meteorological Society*, *132*, 605−623. doi:10.1256/qj.04.182

Healy, S. B., Jupp, A. M., & Marquardt, C. (2005). Forecast impact experiment with GPS radio occultation measurements. *Geophysical Research Letters*, *32*, L03804. doi:10.1029/2004GL020806

INRIA (2002). Software TAPENADE inria 2002, version 2.0, Tech. rep., Domaine de Voluceau, Rocquencourt-BP 105, 78153 Le Chesnay Cedex, France.

IPCC (2007). *Climate change 2007, contribution of WG I and WGII to the 4th Assessment Report of the IPCC.* Cambridge: Cambridge University Press.

Jensen, A. S., Lohmann, M. S., Benzon, H. -H., & Nielsen, A. S. (2003). Full spectrum inversion of radio occultation signals. *Radio Science*, *38*(3), 1040. doi:10.1029/2002RS002763

Kållberg, P., Simmons, A., Uppala, S., & Fuentes, M. (2004). *The ERA40 Archive. ERA40 Project Report Series*, *Vol. 17*. Shinfield Park, Reading, RG2 9AX, England: European Centre for Medium Range Weather Forecast.

Kalnay, E. (2003). *Atmospheric Modeling, Data Assimilation and Predictability.* Cambridge University Press.

Kirchengast, G., Steiner, A. K., Foelsche, U., Kornblueh, L., Manzini, E., & Bengtsson, L. (2000). Spaceborne climate change monitoring by GNSS occultation sensors. *Proc. 11th Symp. on Global Change Studies, Amer. Met. Soc. Annual Meeting 2000, Long Beach/CA, U.S.A.* (pp. 62−65).

Kistler, R., Kalnay, E., Collins, W., Saha, S., White, G., Woollen, J., et al. (2001). The NCEP-NCAR 50-Year reanalysis: monthly means CD-ROM and documentation. *Bulletin of the American Meteorological Society*, *82*, 247−268.

Kozo, N. (Ed.). (1997). *Data Assimilation in Meteorology and Oceanography: Theory and Practice, Special Issue of the Journal of the Meteorological Society of Japan*, *Vol. 75,1B*. Meteorological Society of Japan.

Kuo, Y. -H., Sokolovskiy, S. V., Anthes, R. A., & Vandenberghe, F. (2000). Assimilation of GPS radio occultation data for numerical weather prediction. *TAO (Terrestrial, Atmospheric and Ocean Sciences)*, *11*, 157−186.

Kursinski, E. R., Healy, S. B., & Romans, L. J. (2000). Initial results of combining GPS occultations with ECMWF global analyses within a 1DVar framework. *Earth, Planets and Space*, *52*, 885−892.

Leroy, S. S., Anderson, J. G., & Dykema, J. A. (2006). Testing climate models using GPS radio occultation: a sensitivity analysis. *Journal of Geophysical Research*, *111*, D17105. doi:10.1029/2005JD006145

Leroy, S. S., & North, G. R. (2000). The application of COSMIC to global change research. *TAO*, *11*, 187−210.

Loiselet, M., Stricker, N., Menard, Y., & Luntama, J. -P. (2000). GRAS — MetOp's GPS-based atmospheric sounder. *ESA Bulletin*, *102*, 38−44.

Lorenc, A. C. (1992). Analysis methods for numerical weather prediction. *Quarterly Journal of the Royal Meteorological Society*, *112*, 1177−1194.

Löscher, A., Foelsche, U., & Kirchengast, G. (2006). *CHAMP Radio Occultation Data Assimilation into ECMWF Fields for Global Climate Analyses, WegCenter/Uni Graz Technical Report for FFG-ALR No. 2/2006*.

Nocedal, J. (1996). *Large Scale Unconstrained Optimization.* Tech. Report Department of Electrical Engineering and Computer Science: Northwestern University.

Palmer, P., Barnett, J. J., Eyre, J. R., & Healy, S. B. (2000). A non-linear optimal estimation inverse method for radio occultation measurements of temperature, humidity and surface pressure. *Journal of Geophysical Research*, *105*, 17,513−17,526.

Parrish, J., & and, J. C. (1992). The National Meteorological Center's Spectral Statistical-Interpolation Analysis System. *Monthly Weather Review*, *120*(8), 1747−1763.

Pirscher, B., Foelsche, U., Lackner, B. C., & Kirchengast, G. (2007). Local time influence in single-satellite radio occultation climatologies from sun-synchronos and non sun-synchronos satellites. *Journal of Geophysical Research*, *112*, D11119. doi:10.1029/2006JD007934

Poli, P., Joiner, J., & Kursinski, E. R. (2002). 1DVAR analysis of temperature and humidity using GPS radio occultation refractivity data. *Journal of Geophysical Research*, *107*. doi:10.1029/2001JD000935

Retscher, C., Goncalves, P., Brito, F., & Fusco, L. (2006). Grid on-Demand Enabling Earth Observation Applications: The Atmosphere. *Proc Book Grid-Enabling Legacy Applications and Supporting End Users (GELA) Workshop*: IEEE.

Rocken, C., Kuo, Y., Schreiner, W. S., Hunt, D., Sokolovskiy, S., & McCormick, C. (2000). COSMIC system description. *TAO*, *11*(1), 21−52.

Silvestrin, P., Bagge, R., Bonnedal, M., Carlström, A., Christensen, J., Hägg, M., et al. (2000). Spaceborne GNSS radio occultation instrumentation for operational applications. *Proc 13th ION-GPS Meeting 2000, Salt Lake City* USA: UT.

Skamarock, W. C., Klemp, J. B., Dudhia, J., Gill, D. O., Barker, D. M., Wang, W., et al. (2005). *A Description of the Advanced Research WRF Version 2, NCAR/TN-468+STR, NCAR TECHNICAL NOTE, Mesoscale and Microscale Meteorology Division* Boulder, Colorado, USA: National Center for Atmospheric Research.

Sokolovskiy, S., & Hunt, D. (1996). Statistical Optimization Approach for GPS/Met Data Inversions. *Proc URSI/GPS/Met Workshop, Tucson Arizona*.

Steiner, A. K., & Kirchengast, G. (2005). Error analysis for GNSS radio occultation data based on ensembles of profiles from end-to-end simulations. *Journal of Geophysical Research*, *110*, D15307. doi:10.1029/2004JD005251

Steiner, A. K., Kirchengast, G., Foelsche, U., Kornblueh, L., Manzini, E., & Bengtsson, L. (2001). GNSS occultation sounding for climate monitoring. *Physics and Chemistry of the Earth. Part A: Solid Earth and Geodesy*, *26*, 13−124.

Wickert, J. (2002). *Das CHAMP-Radiookkultationsexperiment: Algorithmen, Prozessierungssystem und erste Ergebnisse.* Tech. Rep. Scientific Technical Report STR02/07 Germany: GeoForschungsZentrum Potsdam.

Wickert, J., Reigber, C., Beyerle, G., Konig, R., Marquardt, C., Schmidt, T., et al. (2001). Atmosphere sounding by GPS radio occultation: first results from CHAMP. *Geophysical Research Letters*, *28*, 3263−3266.

Wickert, J., Schmidt, T., Beyerle, G., König, R., Reigber, C., & Jakowski, N. (2004). The radio occultation experiment aboard CHAMP: operational data analysis and validation of vertical atmospheric profiles. *Journal of the Meteorological Society of Japan*, *82*, 381−395.

Zhu, C., Byrd, R. H., Lu, P., & Nocedal, J. (1995). *L_BFGS_B Fortran Subroutines for Large Scale Bound Constrained Optimization, L BFGS B_ FORTRAN sub routines for large scale bound constrained optimization.* Tech. Report Department of Electrical Engineering and Computer Science: Northwestern University.

Zupanski, M. (1993). A precondition algorithm for large-scale minimization problems. *Tellus*, *45A*, 478−492.